

12. Coaxial (29) and concentric (30) junctions of donor and acceptor arrays have recently been reported for the molecular design of photoinduced energy and electron-transfer systems, respectively.
13. M. Freitag, Y. Martin, J. A. Misewich, R. Martel, Ph. Avouris, *Nano Lett.* **3**, 1067 (2003).
14. M. E. Itkis, F. Borondics, A. Yu, R. C. Haddon, *Science* **312**, 413 (2006).
15. Y. J. Xing *et al.*, *Appl. Phys. Lett.* **87**, 263117 (2005).
16. A. D. Schwab *et al.*, *Nano Lett.* **4**, 1261 (2004).
17. A. M. van de Craats *et al.*, *Adv. Mater.* **11**, 1469 (1999).
18. M. D. Watson, A. Fechtenkötter, K. Müllen, *Chem. Rev.* **101**, 1267 (2001).
19. A. M. van de Craats *et al.*, *Adv. Mater.* **15**, 495 (2003).
20. C. D. Simpson, J. Wu, M. D. Watson, K. Müllen, *J. Mater. Chem.* **14**, 494 (2004).
21. A. C. Grimsdale, K. Müllen, *Angew. Chem. Int. Ed.* **44**, 5592 (2005).
22. J. P. Hill *et al.*, *Science* **304**, 1481 (2004).
23. W. Jin *et al.*, *Proc. Natl. Acad. Sci. U.S.A.* **102**, 10801 (2005).
24. Y. Yamamoto *et al.*, *Adv. Mater.* **18**, 1297 (2006).
25. R. O. Loutfy, C. K. Hsiao, B. S. Ong, B. Keoshkerian, *Can. J. Chem.* **62**, 1877 (1984).
26. T. Sulzberg, R. J. Cotter, *J. Org. Chem.* **35**, 2762 (1970).
27. Materials and methods are available as supporting material on Science Online.
28. A. Acharya *et al.*, *J. Phys. Chem. B* **109**, 20174 (2005).
29. C. Röger *et al.*, *J. Am. Chem. Soc.* **128**, 6542 (2006).
30. W.-S. Li *et al.*, *J. Am. Chem. Soc.* **128**, 10527 (2006).
31. We thank H. Watanabe and K. Suzuki (Hamamatsu) for the measurements of fluorescence quantum yields and time-resolved fluorescence decay profiles and A. Morishima (JASCO Corporation) for the measurement of diffuse reflectance spectroscopy. N.I. performed TEM; M.T. and T.K. constructed the micrometer-gap electrodes; and A.S., S.S., and S.T. made FP-TRMC measurements.

Supporting Online Material

www.sciencemag.org/cgi/content/full/314/5806/1761/DC1

Materials and Methods

Figs. S1 to S7

References

28 August 2006; accepted 1 November 2006

10.1126/science.1134441

A Clathrate Reservoir Hypothesis for Enceladus' South Polar Plume

Susan W. Kieffer,^{1*} Xinli Lu,¹ Craig M. Bethke,¹ John R. Spencer,² Stephen Marshak,¹ Alexandra Navrotsky³

We hypothesize that active tectonic processes in the south polar terrain of Enceladus, the 500-kilometer-diameter moon of Saturn, are creating fractures that cause degassing of a clathrate reservoir to produce the plume documented by the instruments on the Cassini spacecraft. Advective transport of gas and ice transports energy, supplied at depth as latent heat of clathrate decomposition, to shallower levels, where it reappears as latent heat of condensation of ice. The plume itself, which has a discharge rate comparable to Old Faithful Geyser in Yellowstone National Park, probably represents small leaks from this massive advective system.

Data from the instruments on the Cassini spacecraft (1–6) prompt a major scientific question: What is the reservoir that produces the plume on Enceladus? The plume erupts from the tectonically active (1) and warm (2) south polar terrain (SPT); it contains not only H₂O vapor and ice particles (1) but also CH₄, N₂, and CO₂ gases (6). A highly variable flux of the order of 10⁻⁷ to 10⁻⁶ kg s⁻¹ m⁻² (and possibly several orders of magnitude greater, depending on vent conditions at depth) emanates from at least 17 separate vents along the four tectonically active tiger stripes (6, 7). The surface of Enceladus in the SPT is composed of amorphous and crystalline water ice with traces of complexed CO₂ (4).

On the basis of the assumption that the reservoir for the plume is a single-component H₂O system, it was hypothesized that the plume erupted from chambers of liquid water at 273 K as close as 7 m to the surface, the “Cold Faithful” model (1). However, it has also been argued that the plume composition represents the surface and near-surface composition at the site of outgassing

(6), in which case the additional gases must be accounted for. Observed CO₂ concentrations could be in aqueous solution at pressures greater than ~24 bars and could help drive geyser eruptions [as on Earth (8–10)]. However, CH₄ and N₂ are so sparingly soluble in liquid water that these gases could not have originated from a liquid aqueous phase. The solubility of these gases in clathrate hydrates (ices with a cage-like structure in which water ice traps other volatile components), however, is enormous compared with their solubility in liquid water. The observed molar ratio of H₂O vapor to noncondensable gases in the plume is 10:1 (6). The similarity between this and the ratio of water to guest molecules in a clathrate (hydration number is 6:1 to 8:1) suggests that the reservoir could consist of clathrates or clathrates plus water ice. The potentially important role of multicomponent clathrates in Enceladus has been pointed out (11, 12); we investigated the possibility that explosive decomposition of a clathrate of this composition could account for the observations summarized above. Relevant decomposition curves for the binary clathrates and a mixed clathrate of the composition corresponding to the plume are shown in Fig. 1A.

In an undisturbed cold region of Enceladus, including undisturbed regions of the SPT, a conductive geotherm centered at the surface temperature (70 to 80 K, Fig. 1B, point A) would intersect either the CO₂ sublimation curve (Fig. 1B, point B) or the clathrate decomposition curve

(Fig. 1B, point C) before intersecting the H₂O boiling curve (Fig. 1B, point D). Conductive geotherms centered at higher heat flow regions (Fig. 1B, point E) intersect the boiling curve at tens of meters (Fig. 1B, points near F) but are irrelevant if thermal conduction in pure H₂O ice is not the dominant process of heat transport, which we suggest is the case (Fig. 1B, point D).

Water ice and complexed CO₂ have been detected on the surface of Enceladus (4). This observation, coupled with an examination of the phase diagrams of Fig. 1, suggests that the crust consists of a leaky H₂O-CO₂ ice cap “seal” on the order of 3.5-km thickness overlying a clathrate reservoir (13) (Fig. 1B). As long as the seal contains only minor leaks, confining pressure is maintained and the clathrate remains stable. Small leaks will tend to be self-sealing, because water vapor rising from depth freezes in the cold ice cap (Fig. 2A). If the seal breaks and confining pressure is lost, as happens repeatedly as the tectonically active cap fractures, the clathrate is exposed to near-vacuum conditions and decomposes, perhaps violently (Fig. 2, B to D). With time, self-sealing resumes, and the system returns to ambient conditions. In this way, vents in Enceladus' ice cap may be opening and closing continually, producing variable fluxes and plumes that reach high above the moon's surface.

We suggest that episodic and frequent formation of new fractures in the SPT repeatedly exposes clathrate reservoirs to near-vacuum conditions. Large fluxes of gas release are always accompanied by massive ejection of ice grains when decompression takes place (14, 15). As these authors discuss, decomposition may be complicated by the low-temperature polymorphic (hexagonal, cubic, amorphous, and nanophase) changes in ice, but these complexities cannot be addressed quantitatively, so we restrict our discussion to clathrate decomposition. We hypothesize that this process produces jets of gas and ice particles in the fractures comparable to jets produced by comets. If the total pressure drops below the vapor pressure of the ice particles, they sublimate to yield water vapor. Whether this occurs at depth in the fracture (Fig. 2B, left) or above the surface in the plume (Fig. 2B, right) depends on the pressure distribution, which we cannot specify.

¹Department of Geology, University of Illinois at Urbana-Champaign, 1301 West Green Street, Urbana, IL 61801, USA. ²Department of Space Studies, Southwest Research Institute, 1050 Walnut Street, Suite 400, Boulder, CO 80302, USA. ³Thermochemistry Facility and Nanomaterials in the Environment, Agriculture, and Technology (NEAT) Organized Research Unit (ORU), University of California at Davis, 1 Shields Avenue, Davis, CA 95616, USA.

*To whom correspondence should be addressed. E-mail: skieffer@uiuc.edu

Clathrate decomposition into a vacuum is self-sustaining, because vapor is the stable phase, but simultaneously self-limiting, because the decomposition is endothermic. In smaller fractures, condensation may lead to rapid self-sealing (Fig. 2A), but in larger fractures condensation may be limited to boundary layers at the walls. Condensa-

tion is accompanied by the delivery of latent heat to the walls. The boundary layer thickness is limited by the rate of heat transfer away from the walls, and the net effect may be that larger fractures remain open. Nevertheless, the ice coating will shut off the supply of gases, and the pressure, even in a deep fracture, may drop toward vacuum conditions.

When it drops to the vapor pressure of ice at the local temperature, sublimation of ice can begin if there is an adequate heat supply (Fig. 2C). The interplay between these various processes and active tectonics will result in complex and constantly changing fracture networks (Fig. 2D) and could lead to the highly time variable phenomena observed for the plume. We examined whether the magnitudes of the observed gas and vapor fluxes are consistent with the observed thermal constraints and properties of clathrates and ice. Construction of detailed models is neither possible nor warranted by the data available. We could, however, look at two extreme cases: decomposition into a vacuum and into a network of cracks and fractures.

A maximum rate of clathrate decomposition into a vacuum can be calculated from the Hertz-Knudsen-Langmuir equation (16). For decomposition of the mixed clathrate at 190 K and 0.5 MPa, the limiting rate would be $\sim 900 \text{ kg s}^{-1} \text{ m}^{-2}$. An eruption of this magnitude would pose a notable problem to a spacecraft in low orbit but is unlikely to be maintained long enough for Cassini to have encountered such an event during the short time of observations to date. Rather, we assumed that the Cassini measurements are monitoring lower, more steady-state output from the plumes.

To examine decomposition of clathrate into a network of cracks, we adapted the model (17) for depressurization of methane clathrates to gas plus liquid water under terrestrial conditions for decomposition of our hypothesized mixed clathrate to gas plus water ice on Enceladus. The model provides the production rate of the noncondensable gases, which can be tested against the observed fluxes. From the gas flux, estimates of water vapor flux can be made for certain conditions.

The reservoir is represented as a fractured permeable medium. It may be the clathrate itself or a mixture of clathrate and ice or some other solid substance (Fig. 2). Penetration of a fracture initiates a decomposition front that propagates away from the fracture into the clathrate reservoir. Along this front, clathrates decompose at a pressure, P_d , intermediate between the reservoir pressure, P_r , and gas pressure, P_g , in the fracture. Gas production rate is a function of these pressures, temperature, zone permeability, and porosity. We assumed that the heat required for the decomposition 28 kJ mol^{-1} (gas mixture) is available as discussed below. Two plausible cases are discussed; sensitivity studies about the effect of porosity and permeability are provided in Fig. 3 [Supporting Online Material (SOM) text and fig. S1].

We calculated fluxes for one shallow and one deep reservoir to set pressure-temperature boundary conditions. Our nominal shallow cool reservoir has a temperature of 190 K, which is close to that inferred for warm areas (2) and ensures there is sufficient enthalpy to accelerate particles to escape velocity if decompressed to 145 K. For the shallow reservoir, we assigned an initial pressure just high enough for clathrate stability at 190 K, 5 bar. We also examined flow from a deeper reservoir at 35 km (41 bar), corresponding to a

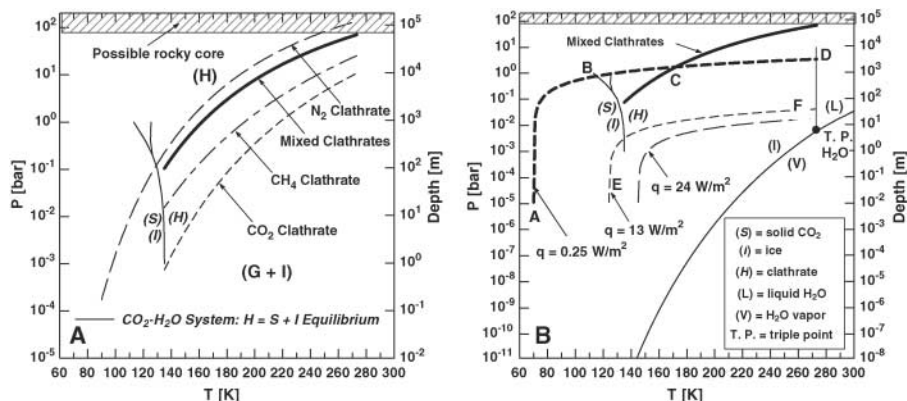


Fig. 1. (A) Decomposition curves from clathrate hydrate (H) to gas plus ice (G+I) for the three binary clathrates of interest and for the mixed clathrate proposed for the reservoir on Enceladus (21, 22) and the sublimation curve for CO_2 (23). (B) Phase relations for H_2O and CO_2 single-component systems, the mixed clathrate system from (A), and some possible shallow thermal profiles. The thermal profile ABC shown is a purely conductive profile for a surface temperature at 1-cm depth of 70 K and a heat flow of 0.25 W m^{-2} . At ambient background conditions on Enceladus, a conductive thermal profile for a density of 1000 kg m^{-3} allows ice to be stable to 3.5 bars pressure and about 3 km depth or the mixed clathrate to be stable at pressure > 1.5 bars (>1.3 km depth). Italicized letters apply only to the CO_2 system.

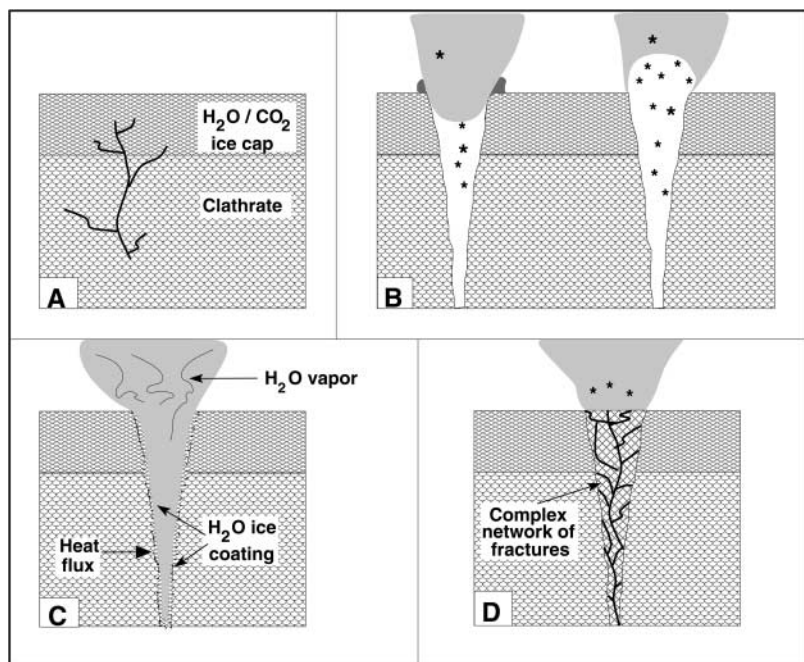


Fig. 2. Schematic illustrations. (A) Small self-sealing fractures extending from the clathrate reservoir through the ice cap seal. (B) A large fracture venting gas plus ice particles derived from the decomposing clathrate directly to the surface. The white area with snowflakes is composed of the noncondensable gases and ice fragments derived from decomposition of the clathrate. The gray area is gas and sublimated water vapor and ice crystals. The birm on the left fracture schematically shows possible surface redeposition from the plume. (C) A fracture into the clathrate with walls coated by H_2O ice, which can sublimate. (D) A complex fracture network through the clathrate and ice. We hypothesize that these variations of fracture geometries and processes are occurring at multiple vents in the SPT and that they are time-variable.

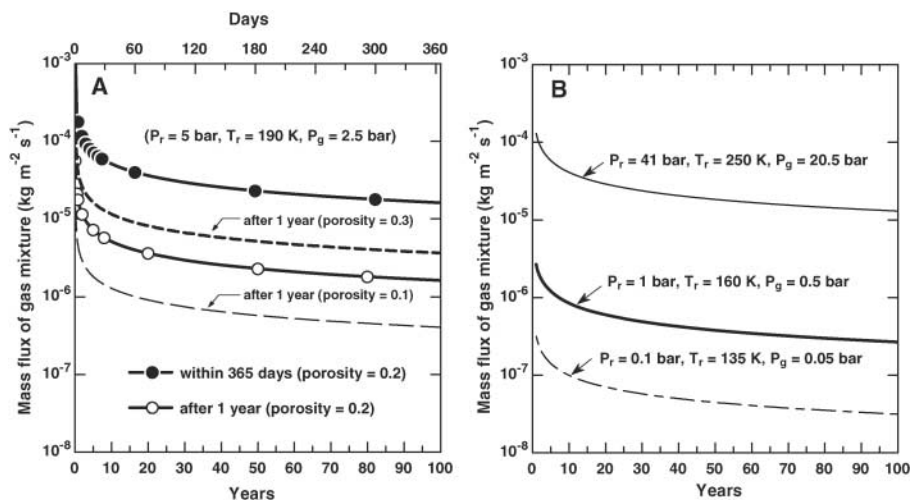


Fig. 3. (A) Flux of noncondensable gases calculated according to the model adapted from (17) on two different time scales (top and bottom axes). The top axis in days applies only to the top curve in this panel of the figure. Sensitivity to porosity shown by dashed curves. (B) Examples of sensitivity to reservoir pressure and temperature.

depth about halfway into the estimated crust, and assigned a temperature of 250 K, corresponding to a plausible geothermal gradient (Fig. 1B). Actual reservoir pressures and temperatures are unknown; these are simply plausible end-members.

Pressures in the active fractures could span the range from reservoir pressure to near-vacuum surface conditions (Fig. 2D). The former is likely at the base of a network of small fractures; the latter, at the base of a single wide fracture. When gas flows in complicated networks, pressure conditions are commonly determined by narrow constrictions where the flow chokes to sonic conditions of pressure, temperature, and flow velocity (Mach number = 1) (18). Typically, this pressure is about half of the reservoir pressure (see Fig. 3 for values).

For the shallow reservoir, initial fluxes of the noncondensable gases (G) are $\sim 10^{-1}$ kg s⁻¹ m⁻² but decrease to $\sim 10^{-4}$ kg s⁻¹ m⁻² within weeks (Fig. 3A), to $\sim 5 \times 10^{-6}$ kg s⁻¹ m⁻² within 10 years, and to $\sim 10^{-6}$ kg s⁻¹ m⁻² within 100 years. Porosity and permeability change these values by about one-half an order of magnitude. Sensitivity tests at even lower pressures and temperatures show that fluxes are in about the same range (Fig. 3B). Fluxes from the deeper reservoir are more than an order of magnitude greater because of both the larger pressure gradient between the reservoir and the fracture and the higher temperature (Fig. 3B).

This model gives the flux of the noncondensable gases, CO₂, N₂, and CH₄. We suggest that these gases entrain small particles of water ice at about the molar ratio of 10:1 (mass ratio of 6:1) and carry them upward in the flow. Upon encountering pressures lower than the vapor pressure either within the fracture or in the atmosphere, these small particles sublimate to produce the observed vapor-to-gas ratio. Therefore, adding in the water vapor component to the observed mass ratio of 6:1 gives a total flux of vapor plus gas of $\sim 7 \times 10^{-4}$ kg s⁻¹ m⁻² after a few weeks, $\sim 35 \times 10^{-6}$ kg s⁻¹ m⁻²

after a decade, and 7×10^{-6} kg s⁻¹ m⁻² after a century. Given the highly variable fluxes and uncertainties in measurements and modeling, these results imply that clathrate degassing could produce fluxes of the order of magnitude measured for the plume, 10^{-7} to 10^{-6} kg s⁻¹ m⁻². The rapid decay over a time frame of weeks is similar to the time scale of 1 month that was documented as the decay time for a burst of particles into Saturn's E-ring observed in 2004, as well as the time scale in (6). The high fluxes calculated from the model also allow some H₂O and CO₂ to recondense on the walls and near surface to form the low ridges of H₂O with trapped CO₂ observed by (1, 4) (Fig. 2B, left, one schematic rim shown in dark gray).

Alternatively, these calculated fluxes will be reduced by a process known to occur when clathrates degas: Surfaces become coated with water ice, and the reaction slows or ceases (Fig. 2C). In this case, the pressure in the fracture drops to the vapor pressure of the ice, and sublimation can occur if heat is available. After sublimation removes or weakens the ice, the degassing cycle can start again (Fig. 2B).

How much heat is required to produce the plume from the clathrate by this process? We ignored the comparatively small energy required for acceleration and considered larger latent heats of decomposition of the clathrate, ~ 890 kJ kg⁻¹ of noncondensable gas mixture, and the additional heat of sublimation of water ice, ~ 2800 kJ kg⁻¹. For a total vapor flux of 100 to 350 kg s⁻¹, the energy required to produce the plumes is then 0.3 to 0.9 GW, about one-tenth of the 3 to 7 GW radiated from the SPT. This is consistent with our hypothesis that much of the energy of decomposition and sublimation is transported from depth and redeposited at higher levels as heat of condensation of ice and carbon dioxide and that the plume represents small leaks on a massive advection system.

We conclude that Enceladus' south polar plume consists of numerous relatively small leaks tapping a system of advecting gases, ice, and vapor (1, 2, 6, 7). The total discharge of a few hundred kilograms per second from all of the vents contributing to the plume at the south pole of Enceladus is remarkably similar to the discharge of Old Faithful Geyser in Yellowstone National Park (18), but the discharge into a vacuum gives the plume its magnificent height and spread. We emphasize that heat transport is not along thermal profiles determined by the thermal conductivity of ice in these regions but rather by advection of vapor and redistribution of latent heats. As an alternative to the shallow boiling water "Cold Faithful" model (1), we propose that the south pole of Enceladus is a colder world with a "Frigid Faithful" plume emanating from degassing clathrates. This model accounts in a simple and unified way for the gas composition of the plume and the variability of fluxes over space and time. It provides a plausible advective heat transfer process as heat absorbed as latent heat of decomposition of clathrate is redeposited near the surface as latent heat of condensation of ice.

References and Notes

1. C. C. Porco *et al.*, *Science* **311**, 1393 (2006).
2. J. R. Spencer *et al.*, *Science* **311**, 1401 (2006).
3. C. J. Hansen *et al.*, *Science* **311**, 1422 (2006).
4. R. H. Brown *et al.*, *Science* **311**, 1425 (2006).
5. F. Spahn *et al.*, *Science* **311**, 1416 (2006).
6. J. H. Waite Jr. *et al.*, *Science* **311**, 1419 (2006).
7. F. Tian, A. I. F. Stewart, O. B. Toon, K. M. Larsen, L. W. Esposito, in preparation.
8. X. Lu, thesis, University of Auckland, Auckland, New Zealand (2004).
9. X. Lu, A. Watson, A. V. Gorin, J. Deans, *Geothermics* **34**, 389 (2005).
10. X. Lu, A. Watson, A. V. Gorin, J. Deans, *Geothermics* **35**, 409 (2006).
11. J. I. Lunine, D. J. Stevenson, *Astrophys. J. Suppl. Ser.* **58**, 493 (1985).
12. J. S. Kargel, *Science* **311**, 1389 (2006); and references therein.
13. The mixed clathrate decomposition curve was calculated using the formulation of (11, 19).
14. D. Laufer, I. Pat-El, A. Bar-Nun, *Icarus* **178**, 248 (2005).
15. For a summary, H. Hong, M. Pooladi-Darvish, P. R. Bishnoi, *J. Can. Petrol. Technol.* **42**, 45 (2003).
16. J. W. Wilder, D. H. Smith, *J. Phys. Chem. B* **106**, 6298 (2002).
17. C. Ji, G. Ahmadi, D. H. Smith, *Chem. Eng. Sci.* **56**, 5801 (2001).
18. S. W. Kieffer, *Rev. Geophys.* **27**, 28 (1989).
19. S. L. Miller, *Science* **165**, 489 (1969).
20. W. F. Kuhs, B. Chazallon, P. G. Podaelli, F. Pauer, *J. Inclusion Phenom. Mol. Recognition Chem.* **29**, 65 (1997).
21. E. D. Sloan Jr., *Clathrate Hydrates of Natural Gases* (Marcel Dekker, New York, ed. 2, 1997).
22. Nitrogen data from (20); methane and carbon dioxide from (21).
23. J. Longhi, *J. Geophys. Res.* **111**, E06011 (2006).
24. We thank P. Chakraborty and G. Gioia for many helpful discussions and acknowledge support by NASA grant NAG5-12747 to S.W.K.

Supporting Online Material

www.sciencemag.org/cgi/content/full/314/5806/1764/DC1
SOM Text
Fig. S1

7 August 2006; accepted 27 October 2006
10.1126/science.1133519